close to the fault [*Catalog of Strong Shocks of China* (Institute of Geophysics Academia Sinica, Beijing, People's Republic of China, 1976)]. Only the 1951 event may be inferred with confidence to correspond to slip on the fault, in view of its focal mechanism (*1*).
4. Molnar and others [P. Molnar *et al.*, *Geology* **15**, 249 (1987); P. Molnar *et al.*, *Science* **235**, 299 (1987)] found large mole tracks and 10-m offsets that they relate to a large earthquake in the last few hundred years on the Altyn Tagh fault near Mangnai Zhen (90°E, Fig. 1). Our fieldwork in the last 3 years has also revealed old earthquake scarps along the fault near Shibaocheng (96°E, Fig. 1). Measurements of scarp profiles imply ages of a few hundred to more than 1000 years.
5. Inferred values of slip rate on the fault range between millimeters and centimeters per year [Ding Guo Yu, *J. Phys. Earth* **34**, S265 (1986); Ma Xing Yuan, *Lithospheric Dynamic Map of China and Adjacent Seas*, scale 1:2,000,000 (State Seismological Bureau, Beijing, China, 1976)].
6. Operational Navigation Charts G7 and G8, scale 1:1,000,000 (Defense Mapping Agency, ed. 3, St. Louis, 1973).
7. The earth observation satellite SPOT (System Probatoire d'Observation de la Terre) was launched on 22 February 1986 by the Centre National d'Etudes Spatiales, France, on a near-polar, circular sunsynchronous orbit, 832 km above the earth's surface. It began commercial operation in July 1986. The scenes used here, 60 km on a side, were provided by SPOT Image, Toulouse, France.
8. Large features of the topography of western Tibet, including the Karakax trough and the glacial morphology of surrounding mountains are clear on Landsat images of the area; see for instance plates E27 and G26 in N. M. Short and R. W. Blair, Jr., Eds., *Geomorphology from Space* (Library of Congress, Washington, DC, 1986).
9. The north and south facing parts of the scarp are respectively shaded from, and illuminated by, the morning sun, Fig. 2C, left.
10. Detailed images of sites not displayed on the figures of this paper are in G. Peltzer, thesis University of Paris VII (1987) and are available from the authors.
11. G. Peltzer *et al.*, *J. Geophys. Res.* **93**, 7793 (1988).
12. B. Wang and E. Derbyshire, *Geogr. J.* **153**, 59 (1987); E. Derbyshire, *Quat. Sci. Rev.* **6**, 301 (1987); *Glacier Inventory of China*, vol. 1 (Lanzhou Institute of Glaciology and Cryopedology, Academia Sinica, Lanzhou, People's Republic of China, 1980).
13. R. Armijo *et al.*, *J. Geophys. Res.* **91**, 13803 (1986); R. Armijo *et al.*, *ibid.* **94**, 2787 (1989).
14. For example, L. D. Labeyrie, J. C. Duplessy, P. L. Blanc, *Nature* **327**, 477 (1987).
15. We take the age of the onset of the Holocene to be between 8,000 and 12,000 years ago, as in (*11, 13*), because a more precise estimate based on local radiometric dating is not available and unwarranted for our crude estimates.
16. J. B. Minster and T. H. Jordan, *J. Geophys. Res.* **83**, 5331 (1978).
17. We thank SPOT Image, Action Thématique Programmée Télédétection, cosponsored by Centre National de la Recherche Scientifique and Centre National d'Etudes Spatiales, and Programme Tectoscope of Institut National des Sciences de l'Univers for support.

2 June 1989; accepted 11 October 1989.

Structure of a Three-Dimensional, Microporous Molybdenum Phosphate with Large Cavities

ROBERT C. HAUSHALTER,* KARL G. STROHMAIER, FRANK W. LAI

The synthesis, single-crystal x-ray structural characterization, and sorption properties of a microporous molybdenum phosphate, $(Me_4N)_{1.3}(H_3O)_{0.7}[Mo_4O_8(PO_4)_2] \cdot 2H_2O$ (Me, methyl), are presented. The three-dimensional framework is built up from $Mo_4O_8^{4+}$ cubes and PO_4^{3-} tetrahedra that are connected in such a way that large, cation-filled voids are generated; these voids constitute 25% of the volume of the solid. Absorption isotherms for water show the completely reversible uptake of 4 to 5 percent by weight water into the micropores of this compound, which corresponds to 10 to 12 percent by volume.

MICROPOROUS SOLIDS WITH LARGE internal surface areas, such as zeolites (*1*), find use in such diverse processes as ion exchange, catalysis, and separations. Zeolites, as well as other microporous solids such as the aluminophosphates (*2*) and a recently discovered aluminoborate (*3*), contain frameworks made from *p*-block elements with primarily tetrahedral coordination and are synthesized hydrothermally in the presence of a templating cation. Although certain transition elements can replace some of the tetrahedrally coordinated Si, P, or Al in zeolitic type solids (*4*), similar solids with anionic frameworks containing stoichiometric amounts of octahedrally coordinated transition elements and large organic, cation-filled cavities are not known.

A few iron phosphates, which are naturally occurring or isostructural with known mineral frameworks, have been prepared, with water or alkali metals in the tunnels (*5*), but none have demonstrated microporosity. Since we had synthesized and structurally characterized both solid-state alkali metal molybdenum phosphates, such as $Cs_4Mo_8P_{12}O_{52}$ (*6*), $Cs_4Mo_{10}P_{18}O_{66}$ (*7*), and $Cs_3Mo_4P_3O_{16}$ (*8*), as well as hydrothermally prepared species such as the large cluster $[Na_{14}Mo_{24}P_{17}O_{97}(OH)_{31}]^{6-}$ (*9*) and a one-dimensional (1-D) polymer, $[(H_3O)_2NaMo_6P_4O_{24}(OH)_7]^{2-}$ (*10*), the possibility of preparing a 3-D framework containing voids filled with organic cations seemed reasonable. We report the synthesis and characterization of $(Me_4N)_{1.3}(H_3O)_{0.7}[Mo_4O_8(PO_4)_2] \cdot 2H_2O$, **1**, which contains a metal-metal bonded, 3-D molybdenum phosphate framework whose cation-filled voids constitute 25% of the volume of the solid. Compound **1** is microporous and shows the reversible uptake of 4 to 5% (by weight) water into its pores.

The reaction of MoO_3, Mo (<2 μm particle size), H_3PO_4, $Me_4N \cdot OH$, and H_2O in a mole ratio of 5:1:18:7:165 at 200°C for 3 days gives a nearly quantitative yield of single-phase **1** as a dark red-brown, microcrystalline powder. The powder x-ray diffraction pattern of **1** was indexed as body-centered cubic with a = 15.05(2) Å (the parenthetical number is the error in the last digit), and no systematic absences beyond those due to the body-centering were observed. This result suggested that the structure may be a body-centered relative of the primitive cubic structure of $Cs_3Mo_4P_3O_{16}$ (*8*) (space group, $P\bar{4}3m$), whose a axis is one-half that of **1**. Use of the hydrolysis product of $MoCl_4$ in place of MoO_3 and Mo in the hydrothermal synthesis gives **1** in the form of large, red, single crystals that were used for a crystal structure analysis (*11*).

The 3-D framework of **1** is built up from $Mo_4O_8^{4+}$ cubes, which have four molybdenyl groups (Mo = O) and two metal-metal bonds with a Mo–Mo distance of 2.617(2) Å (Fig. 1A), and PO_4^{3-} tetrahedra in a ratio of 1 to 2 in the cubic space group $I\bar{4}3m$. In this space group, the entire anionic framework in the 3408(1) Å^3 cell is described by just five atoms: the Mo, μ^3-O, and molybdenyl O all lie on Wyckoff *g* sites at x,x,z; the P atom on the *d* site ($I\bar{4}$ symmetry) at 1/4,1/2,0; and the μ^2-O on a general position. Each cube has a plane, defined by the surrounding 4/2 phosphate groups (four phosphate groups each shared between two cubes), which is perpendicular to the four molybdenyl Mo–O vectors (Fig. 1, B and C). In the crystals, the $Mo_4O_8^{4+}$ cubes are oriented such that these planes in the z = 0 level are parallel to the (100) plane for the cubes centered around 1/2,0,0 and parallel to the (010) and (001) planes for the cubes centered at 0,1/2,0 and 1/2,1/2,0, respectively (Fig. 2A). At the z = 1/2 level, the phosphate-defined planes for the cubes at 0,0,1/2 and 1/2,0,1/2 are parallel to (001) and (010), respectively (Fig. 2B). This connectivity of the anionic

Exxon Research and Engineering Company, Annandale, NJ 08801.

*To whom correspondence should be addressed.

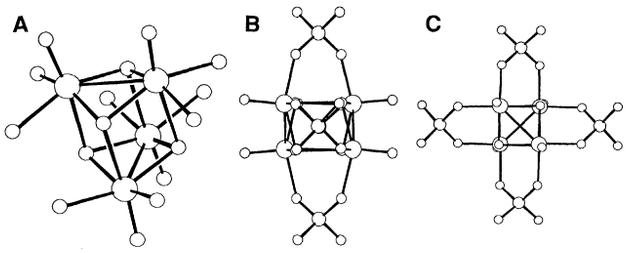

Fig. 1. Representations of (**A**) a $Mo_4O_8^{4+}$ cube with its associated atoms, showing the distorted octahedral coordination of the Mo; (**B**) the $Mo_4O_8(PO_4)_{4/2}$ groups with the plane defined by the four P atoms perpendicular to the plane of the page; (**C**) same as (B) but with the plane parallel to the page. Mo, large circles; P, medium circles; O, small circles.

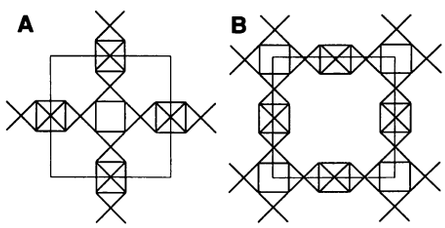

Fig. 2. Schematic illustration of the bonding of the $Mo_4O_8^{4+}$ cubes and phosphate tetrahedra in the (**A**) $z = 0$ and (**B**) $z = 1/2$ levels in **1**.

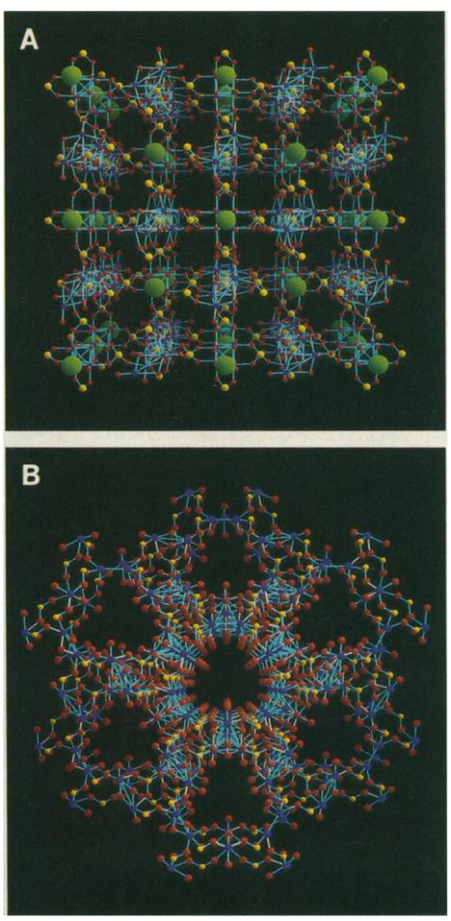

Fig. 3. Chem-X 89 (*18*) representations of the 3-D structure of **1** (Mo, blue; P, yellow; O, red: (**A**) connectivity of the cubes and tetrahedra viewed parallel to [100], emphasizing the ordering of the cation-filled cavities, which are represented as green spheres; (**B**) view parallel to [111], showing the minimum apertures discussed in the text.

framework generates very large cubic-shaped cavities (*12*) centered around 0,0,0 and 1/2,1/2,1/2 as well as tunnels running parallel to ⟨100⟩ and ⟨111⟩ (Fig. 3, A and B).

The framework can also be described in terms of our cubic $Cs_3Mo_4P_3O_{16}$, **2**, structure type (*8*), which has $Mo_4O_4^{6+}$ cubes, with six Mo–Mo bonds and four $Mo^{3.5+}$, connected to other cubes along all crystallographic ⟨100⟩ directions in $P\bar{4}3m$ by 6/2 phosphate groups: removal of one-third of the P atoms and oxidation of the $Mo^{3.5+}$ to Mo^{5+} ($Mo_4P_3O_{16}^{3-}$ to $Mo_4P_2O_{16}^{2-}$) followed by removal of one-fourth of the $Mo_4P_2O_{16}$ units also describes the same structure if the voids are ordered in the proper manner. The ordering of the voids, as well as the orientation of the phosphate-defined planes associated with the $Mo_4O_8^{4+}$ cubes, has been observed in the unique structure type of NbO (*13*), in which the planes defined by the square planar coordination of both the Nb and the O are exactly identical to the planes described above for **1**. Thus both **1** and NbO share the same defect NaCl structure.

The framework composition for the unit cell of **1** is $Mo_{24}P_{12}O_{96}^{12-}$ so that six positive charges are required per cavity. In **1**, the charge balance is achieved with a mixture of Me_4N^+ and H_3O^+ cations, the ratio of which we examined by structural analysis, thermogravimetric analysis (TGA), and elemental analysis. The TGA of **1** under He showed a ~5% weight loss, slightly above 100°C, from the removal of water, and a ~14% weight loss, corresponding to the decomposition of the Me_4N^+ cations, near 425°C, at which temperature the framework apparently collapses. The bulk elemental analysis (*14*) of **1** was also consistent with the presence of a similar percentage (by weight) of Me_4N^+, which, combined with the TGA data, shows the proportions of Me_4N^+:H_3O^+:H_2O to be approximately 2:1:3. This is also in agreement with the results obtained independently from the structural analysis.

To determine if **1** were microporous, that is, if it were possible for small molecules to access all of the internal pore volume, we

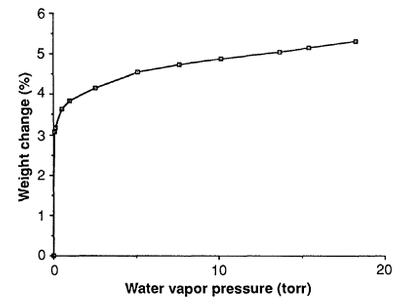

Fig. 4. Absorption isotherm for H_2O and dehydrated, degassed **1** (125°C, 12 hours, 10^{-3} torr) measured at 25°C, demonstrating the zeolitic type of absorption of the water into the micropores.

measured water absorption isotherms on material degassed at 125°C under vacuum. The weight of water absorbed into the degassed solid as a function of the water vapor pressure is plotted in Fig. 4. The shape of the absorption isotherm is type 1 (*15*), indicating the absorption of 4 to 5% (by weight) water (in agreement with the TGA and x-ray results) into the micropores of **1**. The maximum free diameter of the windows (limiting aperture) communicating with the large cubic cavities along the direction parallel to ⟨111⟩ (Fig. 3B) is 2.8 Å. Thus water, with an effective kinetic diameter of 2.8 Å (*16*), can readily penetrate the internal volume of crystals of **1**; however, both dinitrogen (kinetic diameter, 3.8 Å) and *n*-hexane were excluded, according to surface area measurements. The Me_4N^+ cations were still present in the cavities when the water sorption measurements were performed.

The synthesis of **1** shows that it is possible to prepare, simply and in high yield, a microporous, three-dimensional (3-D), mixed octahedral-tetrahedral, transition-metal, main-group oxide framework containing large cation-filled voids. Other hydrothermally prepared molybdenum phosphates with two-dimensional layered structures have been prepared and will be reported elsewhere (*17*).

REFERENCES AND NOTES

1. R. M. Barrer, *Hydrothermal Chemistry of the Zeolites* (Academic Press, London, 1982).
2. S. T. Wilson, B. M. Lok, C. A. Messina, T. R. Cannan, E. M. Flannigan, *J. Am. Chem. Soc.* **104**, 1146 (1982).
3. W. Jianhua, F. Shouhua, X. Ruren, *Chem. Commun.* **1989**, 5265 (1989).
4. E. M. Flanigen, B. M. Lok, R. L. Patton, S. T. Wilson, *Pure Appl. Chem.* **58**, 1351 (1986).
5. P. B. Moore and S. Chen, *Nature* **306**, 356 (1983); D. R. Corbin *et al.*, *Inorg. Chem.* **25**, 2279 (1986).
6. K. H. Lii and R. C. Haushalter, *J. Solid State Chem.* **69**, 320 (1987).
7. R. C. Haushalter and F. W. Lai, *ibid.* **76**, 218 (1988).
8. R. C. Haushalter, *Chem. Commun.* **1987**, 374 (1987).
9. ——— and F. W. Lai, *Angew. Chem.* **101**, 802 (1989).
10. ———, *Inorg. Chem.* **28**, 2904 (1989).

11. Crystal data for 1: cubic, space group $I\bar{4}3m$ (#217), a = 15.0487(18) Å at −140°C and R factor (weighted R) = 0.026(0.031).
12. Considering the protrusion of the molybdenyl groups into the cubic cavities, the size of the cavities can be estimated as follows. One can obtain a maximum value by taking the cube root of the volume of the cavity obtained from the defect analogy of 1 and NbO (see text), which yields a value of $[0.25(3408)]^{0.33}$ = 9.5 Å. Alternatively, one can derive a minimum value by subtracting the appropriate bond lengths from the unit cell edge: two times the molybdenyl Mo–O distance plus two times the Mo–O trans to the molybdenyl group plus one oxygen diameter, which gives 1.6 + 2.4 + 2.8 = 6.8 Å, but this estimate does not include the volume in the "corners" of the cubic cavities between the protruding molybdenyl groups.
13. A. L. Bowman, *Acta Crystallogr.* **21**, 843 (1966).
14. Because the total amount of organic cation present as determined from the x-ray data was in agreement with the results of the elemental analysis, we used the N:Mo ratio from the x-ray analysis to determine the calculated empirical formula of 1: calculated for anhydrous $[(Me_4N)_{1.33}(H)_{0.67}][Mo_4P_2O_{16}]$: C, 7.98%; H, 2.12%; N, 2.32%; P, 7.74%; and Mo, 47.97%; found: C, 8.50%; H, 2.51%, N, 2.31%; P, 7.43%; and Mo, 47.30%.
15. D. M. Ruthven, *Principles of Adsorption and Adsorption Processes* (Wiley, New York, 1984), p. 49.
16. D. W. Breck, *Zeolite Molecular Sieves* (Wiley-Interscience, New York, 1974), p. 636.
17. E. W. Corcoran, Jr., unpublished results; R. C. Haushalter and L. Mundi, unpublished results.
18. Chem-X, Chemical Design, Ltd., Mahwah, NJ.
19. We are grateful to H. G. von Schnering for pointing out several important features of the structure, for noting the similarity between the vacancy ordering in this structure and that of NbO, and for many useful discussions.

6 July 1989; accepted 2 October 1989

Spatial Patterns from Oscillating Microtubules

ECKHARD MANDELKOW, EVA-MARIA MANDELKOW, HIROKAZU HOTANI, BENNO HESS, STEFAN C. MÜLLER

Microtubules are fibers of the cytoskeleton involved in the generation of cell shape and motility. They can be highly dynamic and are capable of temporal oscillations in their state of assembly. Solutions of tubulin (the subunit protein of microtubules) and guanosine triphosphate (GTP, the cofactor required for microtubule assembly and oscillations) can generate various dissipative structures. They include traveling waves of microtubule assembly and disassembly as well as polygonal networks. The results imply that cytoskeletal proteins can form dynamic spatial structures by themselves, even in the absence of cellular organizing centers. Thus the microtubule system could serve as a simple model for studying pattern formation by biomolecules in vitro.

THE SELF-ASSEMBLY OF BIOPOLYMERS from their subunits is usually described in terms of the helical condensation theory (*1*). The model contains the phases of nucleation, followed by elongation of subunits onto the polymer ends until a steady state of assembly is attained. The model also assumes a homogeneous distribution of all reacting species. In the case of microtubules, the simple condensation model was superseded by that of dynamic instability (*2*), where—even at steady state—some polymers grow while others shrink. Microtubules are the only biopolymers known that exhibit this unusual behavior; it depends on the hydrolysis of GTP that accompanies microtubule assembly. One can even synchronize an entire population of microtubules so that they grow or shrink simultaneously; this leads to oscillations in the level of assembly that can be observed by light or x-ray scattering (*3–6*). The mechanism of oscillations proposed previously (*5, 6*) contains the following steps. Microtubules are formed from their subunits tubulin (Tu) with bound GTP (Tu·GTP); GTP is hydrolyzed during assembly, leading to the destabilization of microtubules; microtubules depolymerize into tubulin oligomers which contain bound GDP (guanosine diphosphate); oligomers dissociate into tubulin with bound GDP (Tu·GTP); and GDP is replaced by GTP from the solution so that assembly-competent Tu·GTP is regenerated. Since the dissolution of oligomers is slow they can be regarded as a "refractory" state. The transition from microtubule growth to shrinkage can be modeled by cooperativity between tubulin subunits on microtubule ends. Computer simulations show that this model can explain the observed homogeneous oscillations, but it does not predict spatial patterns.

Whereas previous reports (*3–6*) have dealt with the case of spatially homogeneous oscillations, we now give an example of an inhomogeneous oscillation generating a simple spatial pattern (Fig. 1). A cold tubulin solution (0°C) was filled into a cuvette thermostatted at 37°C. After a lag of about 30 s, microtubules assemble and oscillate with a periodicity of 210 s. However, different parts of the solution oscillate with a shift in phase so that waves of assembly and disassembly appear to be rolling from the top to the bottom of the tube. This behavior is not due to a gradient in temperature because this equilibrates within a few seconds, well before the onset of assembly.

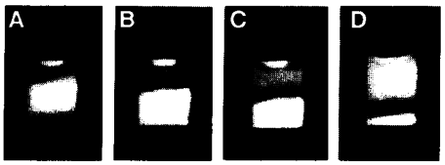

Fig. 1. Light scattering of oscillating microtubules. The reaction was started by filling 200 μl of the cold protein solution in a cuvette thermostatted at 37°C; the images were taken (**A**) 532, (**B**) 555, (**C**) 605, and (**D**) 655 s after the temperature jump. The light scattering indicates microtubule assembly. An assembly wave moves from top to bottom at about 0.015 mm/s. The width of the cell is 4 mm. Tubulin was purified from porcine brain as described (*6*). Oscillations were obtained at high protein concentrations (typically 10 to 50 mg/ml) in various buffer conditions, for example 0.1*M* Pipes (1,4-piperazinediethanesulfonic acid), *p*H 6.9, 20 m*M* $MgSO_4$, 60 m*M* NaCl, 1 m*M* EGTA, 1m*M* dithiothreitol, and 6 m*M* GTP.

More detailed information can be obtained by a two-dimensional ultraviolet (UV) spectrophotometer designed to study the Belousov-Zhabotinskii (BZ) reaction (*7*). In Fig. 2 results are shown for an experiment in which the cold protein solution was filled into a thermostatted petri dish so that the final temperature of about 37°C was reached within a few seconds. The reaction started after a lag time of about 30 s; it was observed by the transmitted intensity of a parallel beam of UV light (390 nm) recorded on a TV detector. One observes concentric rings of high scattering (green to light blue in the color coding of Fig. 2, A through C) typically a few millimeters wide, originating at the periphery and traveling toward the center where they disappear. As in Fig. 1, the scattering is due to microtubule assembly; the periodicity of the waves is of the same order as that of the homogeneous microtubule oscillations described previously, that is, about 1 to 3 min, depending on buffer conditions. Similar observations can be made in reflected light by time-lapse cinematography (Fig. 2, D through F), except that the contrast is reversed. During an experiment the frequency of wave generation at the periphery remains roughly constant, but the speed of propagation toward the center tends to decrease. As a result the number of visible wave crests increases with time (Fig. 2, A through C).

The patterns described above are easily seen by eye, but there are two other types of patterns visible only a higher resolution in

E. Mandelkow and E.-M. Mandelkow, Max-Planck-Unit for Structural Molecular Biology, c/o DESY, Notkestrasse 85, D-2000 Hamburg 52, West Germany.
H. Hotani, ERATO, Molecular Dynamic Assembly Project, 15 Morimoto-cho, Shimogamo, Kyoto 606, Japan.
B. Hess and S. C. Müller, Max-Planck-Institut für Ernährungsphysiologie, Rheinlanddamm 201, D-4600 Dortmund 1, West Germany.